



# Interregional neural synchrony has similar dynamics during spontaneous and stimulus-driven states

Avniel Singh Ghuman, Rebecca N. van den Honert & Alex Martin

Laboratory of Brain and Cognition, National Institute of Mental Health, National Institutes of Health, Bethesda, MD, United States.

SUBJECT AREAS:

CORTEX

SOMATOSENSORY SYSTEM

CONSCIOUSNESS

ATTENTION

Received  
26 October 2012

Accepted  
7 February 2013

Published  
19 March 2013

Correspondence and requests for materials should be addressed to A.S.G. (ghumana@upmc.edu)

Assessing the correspondence between spontaneous and stimulus-driven neural activity can reveal intrinsic properties of the brain. Recent studies have demonstrated that many large-scale functional networks have a similar spatial structure during spontaneous and stimulus-driven states. However, it is unknown whether the temporal dynamics of network activity are also similar across these states. Here we demonstrate that, in the human brain, interhemispheric coupling of somatosensory regions is preferentially synchronized in the high beta frequency band (~20–30 Hz) in response to somatosensory stimulation and interhemispheric coupling of auditory cortices is preferentially synchronized in the alpha frequency band (~7–12 Hz) in response to auditory stimulation. Critically, these stimulus-driven synchronization frequencies were also selective to these interregional interactions during spontaneous activity. This similarity between stimulus-driven and spontaneous states suggests that frequency-specific oscillatory dynamics are intrinsic to the interactions between the nodes of these brain networks.

Neurons, *in vivo*, are active in the absence of external input. Increasing evidence suggests that this spontaneous activity has a coherent structure and may play a role in a host of cognitive and neural processes, such as motor performance<sup>1</sup>, learning and memory<sup>2</sup>, and neural development<sup>3</sup>. In support of this possibility, recent neurophysiological studies have shown that the activity of individual neurons is similar across spontaneous and stimulus-driven brain states<sup>4–8</sup> and a recent transcranial magnetic stimulation study suggested the same<sup>9</sup>. This similar activity has motivated a number of hypotheses about the mechanism by which spontaneous neural activity contributes to cognition<sup>4,6,9–11</sup>.

The neurophysiological evidence from single neurons has been complemented by findings from neuroimaging studies that have revealed a correspondence between spontaneous and stimulus-driven states regarding the spatial structure of large-scale functional networks, consistent with the idea that the brain has an intrinsic functional architecture<sup>12–15</sup>. This spatial correspondence has been based on interregional correlations of spontaneous, slow fluctuations in the brain's hemodynamic activity (< .1 Hz)<sup>12–15</sup> with some evidence that these fluctuations may be associated with gamma band electrophysiological activity (30+ Hz)<sup>16–18</sup> or that the precise frequency associated with these slow fluctuations differ across the brain<sup>19,20</sup>. However, it is unknown whether the frequency bands associated with interregional synchrony during stimulus-driven and spontaneous states of these large-scale interactions are related<sup>9</sup>.

Current evidence suggests that stimulus-driven interregional synchrony is associated with temporal dynamics in a broad range of frequency bands (here termed “oscillatory synchronization”) that may vary as a function of task and brain network. For example, spatial navigation tasks modulate hippocampal neuronal synchrony in the theta frequency band (4–8 Hz)<sup>21</sup>, and median nerve stimulation modulates neural synchrony in the somatosensory cortex in the beta frequency band (13–30 Hz)<sup>22,23</sup>. Here we test the hypothesis that the frequency bands associated with stimulus-driven oscillatory synchronization between specific neural regions are also characteristic of their spontaneous synchrony.

## Results

We used magnetoencephalography (MEG) to compare stimulus-driven and spontaneous oscillatory phase locking<sup>22,24,25</sup> - a measure of the precise temporal synchronization of neural signals - in somatosensory and auditory regions. The regions chosen for phase locking analysis were in different hemispheres of the brain and further than 6 cm apart to avoid potential artifactual crosstalk that occurs between relatively proximal locations in MEG<sup>24</sup>. Data for evaluating stimulus-driven oscillatory synchrony in the somatosensory regions were obtained by having

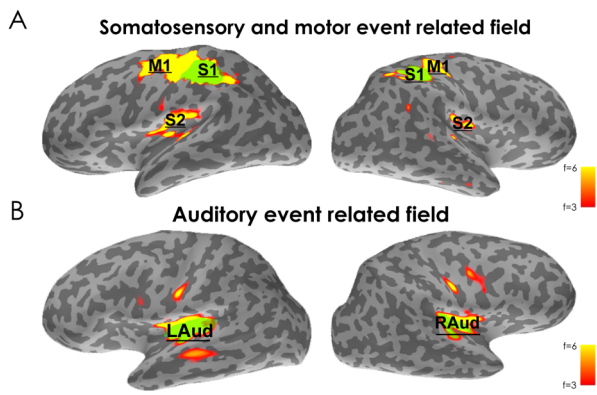


**Figure 1** | (A) Single subject example of the event related fields following a button press with the left index finger (right hemisphere image) or the right index finger (left hemisphere image). Noise normalized, dynamical statistical parametric mapping images are plotted<sup>55</sup>. The regions chosen for LM1, S1, and S2 are labeled. (B) Single subject example of the event related fields during passive listening to auditory clicks. The regions chosen for LAud and RAud are labeled.

subjects ( $N = 10$ ) perform a cued bimanual button press task (see figure 1A for an example event related response to button press). Phase locking was calculated between a region in the right hemisphere primary somatosensory cortex (RS1) and the left hemisphere secondary somatosensory cortex (LS2) identified via analysis of the data from 0–150 ms after the onset of the button press (figure 1A; synchrony between RS1 and LS1 could not be reliably evaluated because they are less than 6 cm apart). Data for evaluating stimulus-driven oscillatory synchrony in the auditory cortices were obtained while subjects passively listened to clicks (15, 20, 30, or 40 Hz, 500 ms duration, interstimulus interval = 1.5 sec) delivered binaurally (see figure 1B for an example event related response to auditory clicks). Phase locking was calculated between left and right hemisphere primary auditory cortices (LAud and RAud), identified via analysis of the passive listening data averaged across all frequency conditions (figure 1B). Data for evaluating spontaneous oscillatory synchrony were obtained by having subjects fixate a centrally located cross for 12 minutes prior to their participation in the button press or passive listening task. Spontaneous phase locking was evaluated between the aforementioned interhemispheric somatosensory and auditory sites during the passive fixation period. All statistical values were based on a permutation test and corrected for multiple frequency comparisons<sup>26</sup>.

**Stimulus-driven and spontaneous synchrony between RS1 and LS2.** In somatosensory cortices, we found increased interhemispheric phase locking between RS1 and LS2 that was restricted to the high beta frequency range during the button press relative to a prestimulus baseline (figure 2A;  $p = .008$  from 20–28 Hz). This finding is consistent with previous studies that demonstrated that phase locking increases in the beta frequency band between RS1 and LS2 following median nerve stimulation<sup>22,23</sup> and reports indicating the importance of beta band synchrony in the sensory-motor system<sup>27–29</sup>. The similarity between our phase locking results to previous reports of synchrony during somatosensory stimulation<sup>22,23</sup> and the time window of analysis (0–150 ms post button press onset) suggest that this RS1-LS2 phase locking reported is a result of proprioception during the button press. Importantly, significantly greater phase locking in the high beta frequency range was also seen for spontaneous activity between these same sites (RS1 and LS2), relative to both noise and the RH motor cortex (RM1)-LS2 control site pair (figure 2B;  $p < .002$  from 22–30 Hz). The largest peak in the RS1-LS2 phase locking occurred in the alpha frequency band, though the synchrony at these frequencies was not significantly different between RS1-LS2 and RM1-LS2. Indeed, the somatomotor rhythms have both alpha and beta frequency components<sup>30</sup> and this alpha synchrony may be involved in somatosensory-motor interactions. It is noteworthy that a peak of phase locking in the high beta frequency band is also visible during the prestimulus period (figure 2A), consistent with the idea that this frequency is important to spontaneous synchrony between RS1 and LS2.

**Stimulus-driven and spontaneous synchrony between RAud and LAud.** A similar pattern of correspondence between the stimulus-driven and spontaneous interhemispheric oscillatory synchrony was found between the auditory sites. Specifically, we found increased phase locking between RAud and LAud that was restricted to the alpha frequency range during the presentation of the clicks relative to a prestimulus baseline (figure 3A;  $p < .05$  from 7–15 Hz). While we are unaware of any previous studies that examined phase locking between RAud and LAud in response to auditory stimulation, previous work has shown that the local neural response in the alpha frequency band in both RAud and LAud is modulated by auditory stimuli<sup>31–33</sup>. These same sites (RAud-LAud) also showed significantly greater phase locking in the alpha frequency range for spontaneous activity, relative to both noise and the RAud-LM1 control site pair (figure 3B;  $p = .006$  from 10–14 Hz). The fact that a peak of phase locking in the alpha frequency band is also visible during the prestimulus period (figure 3A), further supports the idea that this frequency is important to spontaneous synchrony between RAud and LAud.

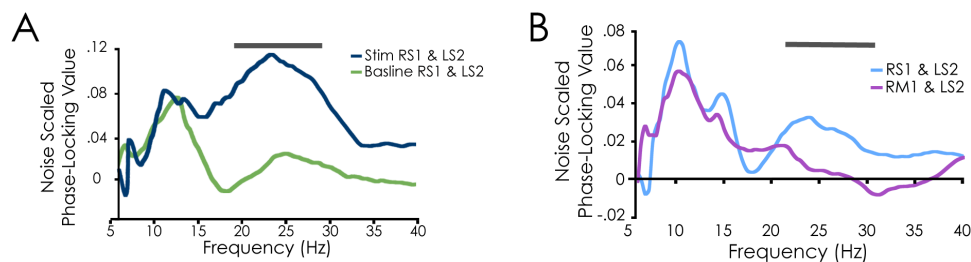


**Figure 2** | **Stimulus-driven and spontaneous synchronization between left and right hemisphere somatosensory cortices.** (A) Phase locking between RS1 and LS2 with respect to frequency during a cued button-press task. The phase locking during the button-press and during the period prior to presentation of the button-press cue (pre-stimulus baseline) is shown. Significantly greater phase locking was seen during the button-press compared to the pre-stimulus baseline period only in the high beta frequency range (20–28 Hz indicated by the grey bar above the data). (B) Spontaneous phase locking between RS1 and LS2 and between RM1 and LS2 (control pair) with respect to frequency. RM1-LS2 were chosen as the control pair because their Euclidean distance is the same as between the RS1-LS2 pair of interest. Significantly greater phase locking was seen for RS1-LS2 versus noise and RM1-LS2 control pair regions only in the high beta frequency range (22–30 Hz indicated by the grey bar above the data).

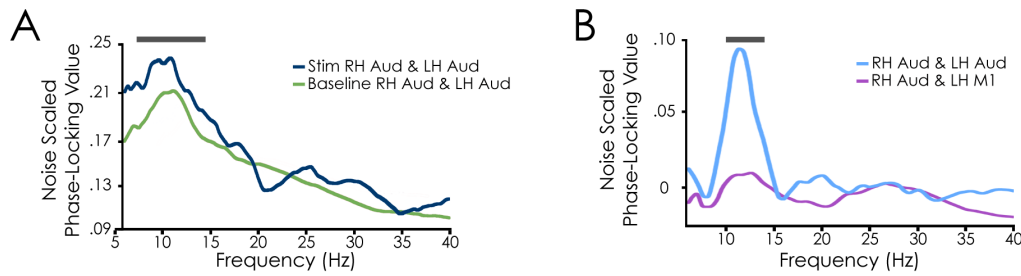


**Figure 3 | Stimulus-driven and spontaneous synchronization between left and right hemisphere auditory cortices.** (A) Phase locking between RAud and LAud with respect to frequency during presentation of auditory clicks and during the period prior to presentation of the clicks (pre-stimulus baseline). Significantly greater phase locking was seen during auditory stimulation compared to the pre-stimulus baseline period only in the alpha frequency range (7–15 Hz indicated by the grey bar above the data). (B) Spontaneous phase locking between RAud and LAud versus between RAud and LM1 (control pair regions) with respect to frequency. RAud-LM1 were chosen as the control pair because their Euclidean distance is the less than the RS1-LS2 pair of interest. Significantly greater phase locking was seen for RAud-LAud than for RAud-LM1 only in the alpha frequency range (10–14 Hz indicated by the grey bar above the data).

**Slow fluctuations of spontaneous synchrony.** These findings establish that the frequencies associated with enhanced, interhemispheric neural synchrony between somatosensory regions due to proprioception during a motor task, and between auditory cortices when listening to clicks, are also critical to spontaneous synchrony within these systems. To address whether our findings might be related to the slow fluctuations ( $< .1$  Hz) of correlated activity seen in neuroimaging studies of spontaneous functional connectivity<sup>12,13,15</sup>, we examined the rate at which this relatively high frequency interregional synchronization varied over time. Specifically, we used a Fourier analysis to examine the rate of change over time of the phase locking at the target frequency of both interhemispheric interactions (figures 4A and 4C). For the two pairs of regions, RS1-LS2 and RAud-LAud, a greater amount of the change over time of the

high beta and alpha phase locking, respectively, was accounted for by lower frequencies than higher frequencies, with the lowest frequencies (e.g.  $< .1$  Hz) accounting for the most variability (RS1-LS2: mean  $R = -.50$ ,  $t = -5.62$ ,  $p < .001$ ; figure 4B; RAud-LAud: mean  $R = -.60$ ,  $t = -13.44$ ,  $p < .001$ ; figure 4D). Thus, spontaneous interregional synchronization between these brain areas is characterized by very slow fluctuations of higher frequency oscillations<sup>19,20,34</sup>. Critically, these higher frequency oscillations are the same for stimulus-driven and spontaneous synchrony.

One question is whether these slow fluctuations of higher frequency phase locking are primarily driven by the regions slowly coupling and decoupling or whether they are governed by increases and decreases in local activity. While increases and decreases in local activity do not directly affect phase locking, they modulate the

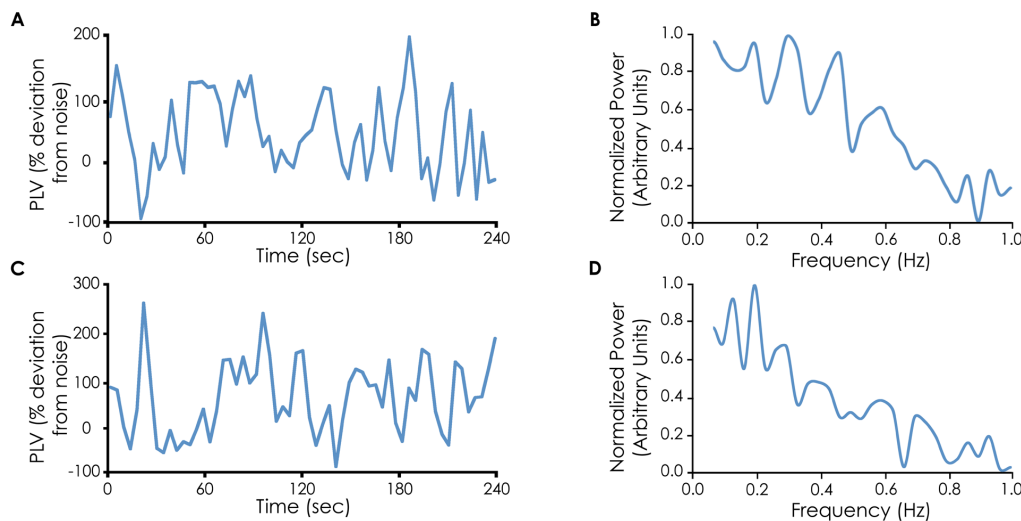


**Figure 4 | (A)** Spontaneous time courses of the 24 Hz phase locking between RS1 and LS2 for a representative subject. As illustrated, synchrony (phase-locking values) fluctuated very slowly over time (on the order of secs). Phase locking is plotted relative to the average of 1000 noise simulations using random, Gaussian-distributed noise. **(B)** The Fourier spectrum of the 24 Hz synchrony between RS1 and LS2. Power increased linearly from the highest to the lowest frequencies. A significant ( $p < .01$ ) negative linear relationship between frequency and power was seen in 8/10 subjects with an overall highly-significant relationship across subjects (mean  $R = -.50$ ,  $t = -5.62$ ,  $p < .001$ ). Furthermore, the slope of the 24 Hz spectrum was significantly steeper (more negative) than random noise ( $t = -2.14$ ,  $p = .03$ ) while the 18 Hz spectrum (not pictured) did not differ from noise ( $t = -1.31$ ,  $p > .1$ ) indicating that the high beta frequency synchrony between RS1 and LS2 fluctuates very slowly. **(C)** Spontaneous time courses of the 10 Hz phase locking between RAud and LAud for a representative subject illustrating that the synchrony varied slowly over time. **(D)** The Fourier spectrum of the 10 Hz synchrony between RAud and LAud. As in panel B, power increased linearly from the highest to the lowest frequencies, and there was a significant negative linear relationship between frequency and power in 9/10 subjects with an overall highly-significant relationship across subjects (mean  $R = -.60$ ,  $t = -13.44$ ,  $p < .001$ ). Also, the slope of the 10 Hz spectrum was significantly steeper than random noise ( $t = -3.03$ ,  $p = .007$ ) while the 20 Hz spectrum (not pictured) was not ( $t = -0.99$ ,  $p > .1$ ) indicating that the alpha frequency synchrony between RAud and LAud changes very slowly. Note that while the data B and D were well fit by a negative linear relationship, they were also well fit by a 1/frequency relationship.



signal-to-noise ratio, which does affect measures of phase locking<sup>35,36</sup>. To address this question we examined the correlation over time between local power and phase locking. A significant correlation was seen between RS1 power and RS1-LS2 phase locking at 24 Hz (mean  $R = .17$ ,  $t = 8.32$ ,  $p < .001$ ), LS2 power and RS1-LS2 phase locking at 24 Hz (mean  $R = .13$ ,  $t = 3.23$ ,  $p < .05$ ), RAud power and RAud-LAud phase locking at 10 Hz (mean  $R = .12$ ,  $t = 3.14$ ,  $p < .05$ ), and LAud power and RAud-LAud phase locking at 10 Hz (mean  $R = .20$ ,  $t = 16.4$ ,  $p < .001$ ). Additionally, the RS1 and LS2 power-phase locking correlations were significantly greater at 24 Hz than at 18 Hz ( $p < .01$  in both cases) and the RAud and LAud power-phase locking correlations were significantly greater at 10 Hz than at 20 Hz ( $p < .005$  in both cases). Finally, it should be noted that the power correlation between RS1 and LS2 at 24 Hz was not significantly larger than at 18 Hz ( $t = 1.91$ ,  $p = .09$ ) nor was the power correlation between RAud and LAud at 10 Hz significantly larger than at 20 Hz ( $t = 2.03$ ,  $p = .07$ ), though both showed a trend towards significance. These results demonstrate that some of the fluctuations over time of the interregional phase locking can be explained by increases and decreases in the local power in the respective areas. However, the correlation coefficients do not exceed .20, indicating that these local changes do not explain a substantial proportion of the variance ( $< 5\%$ ) of the phase locking over time. Thus, our results suggest that RS1-LS2 and RAud-LAud slowly go in and out of synchrony during the spontaneous state at 24 Hz and 10 Hz respectively, at least partially independent of local activity changes.

## Discussion

Our results suggest that activity in the same frequency bands underlies interregional synchrony for both stimulus-driven and spontaneous brain states. Specifically, increased interhemispheric phase locking in the beta frequency band between RS1 and LS2 and in the alpha frequency band between RAud and LAud was associated with somatosensory and auditory response respectively. Furthermore, interhemispheric phase locking in these same frequency bands was characteristic of spontaneous communication between these regions. This correspondence between stimulus-driven and spontaneous oscillatory synchronization suggests that the dynamics are not purely state dependent, appearing and disappearing as needed. Rather, our results suggest that the dynamics at these frequencies are intrinsic to these interregional interactions.

In support of the hypothesis that frequency specific synchrony is intrinsic to interregional interactions, physiology and neural modeling suggests that relatively stable properties of neural regions, such as different conduction delays between brain regions and other network properties can guide oscillatory dynamics<sup>37–40</sup>. One putative role for these intrinsic dynamics is to allow for dynamic control over how and where information is gated<sup>38,41</sup>. Further studies will be required to determine whether frequency specific oscillatory dynamics extend beyond interhemispheric coupling of early sensory cortices.

The present results suggest that interacting brain regions spontaneously synchronize in particular frequency bands and that stimulus-driven activity increases the interregional synchrony at that frequency. These intrinsic oscillatory dynamics are generally consistent with the hypothesis that stimulus-driven activity can be described as a perturbation of the ongoing, spontaneous electrophysiological brain activity<sup>11,42</sup>. Most previous studies have examined these perturbations relative to the prestimulus period (i.e. in the context of the task or stimulus). The similarity between the prestimulus baseline and the spontaneous activity seen in the present results extend this framework beyond a task or stimulus context to the resting-state. Furthermore, most previous studies have examined these perturbations in local neural activity<sup>11,43</sup>. Our results suggest that a similar mechanism may underlie interregional synchrony at the intrinsic oscillatory frequencies described here.

This is not meant to imply that all types of oscillatory synchrony are intrinsic to particular brain interactions. For example, gamma frequency dynamics are seen ubiquitously throughout the brain. Gamma synchrony is associated with distinct cognitive states such as attention<sup>44</sup>, learning<sup>45</sup>, and working memory<sup>46</sup>, processes that inherently involve many brain networks. Thus, networks may be partly characterized by intrinsic oscillatory mechanisms while also being subject to transient or global oscillatory states. Indeed, dynamics in multiple oscillatory frequencies can exist within networks and often interact with one another, leading to frequency nesting and cross-frequency interactions<sup>47,48</sup>.

It is unclear how the present results relate to previous reports emphasizing the role of gamma band oscillations in slow spontaneous activity<sup>16–18</sup> because these previous studies did not directly compare stimulus-driven and spontaneous synchrony as was done here. The present results demonstrate that the spontaneous state is characterized by slow changes in higher frequency synchrony, and that these higher frequency dynamics are similar in stimulus-driven and spontaneous states. At long time-scales, this result is consistent with neuroimaging studies showing that spontaneous activity is characterized by slow fluctuations of correlated activity<sup>12,13,15</sup>. At relatively brief timescales (on the order of hundreds of milliseconds), this result is also consistent with neurophysiological evidence in animals that show a marked similarity between the temporal structure of spontaneous and stimulus-driven activity at the spatial scale of individual neurons and at the temporal scale of milliseconds<sup>4–8</sup>. Accordingly, the present work bridges the gap between these previously disparate human neuroimaging and animal neurophysiology studies.

Although our data do not address the function of ongoing neural synchrony, one intriguing possibility is that it provides stability to the interregional interactions that underlie brain networks<sup>13</sup>. Consistent with this idea, recent modeling work demonstrates that interregional synchronization can improve a network's resilience against the potentially destabilizing effects of noise<sup>49</sup>. Therefore, sustained oscillatory synchrony may be a way for nodes of a neural network to resist noise in order to maintain coherence and stabilize the information represented in that network.

The present data demonstrate that spontaneous interregional synchrony slowly varies over time (i.e. non-stationarity). These results are generally consistent with previous fMRI<sup>50,51</sup>, MEG<sup>19,20</sup>, and intercranial EEG<sup>16–18</sup> studies showing similar effects. These previous results have looked primarily at whether interregional correlations between the overall level of activity fluctuated over time (though<sup>51</sup> examined slow changes in phase coupling using fMRI as well). Our results demonstrate that the relative phase of the regions also fluctuates slowly over time, with the phase of RS1-LS2 and RAud-LAud slowly coupling and decoupling over the spontaneous period. Furthermore, these changes in phase locking were at least partially independent of local changes in the power of the activity within these regions.

One potential limitation of these data is that the RS1-LS2 stimulus-related synchrony relies on somatosensory proprioception during a motor task. This task may confound motor and somatosensory activity and is not well matched to the passive auditory task used to examine RAud-LAud synchrony. However, previous studies using passive median nerve stimulation have reported increased synchrony specific to the beta-band in these tasks<sup>22,23</sup>, which is consistent with the present results despite the very different tasks. Additionally, it is not clear if the stimulus-related increases in synchrony between RS1-LS2 and RAud-LAud were due primarily to increased coupling between these regions or due to local changes in activity that result from the stimuli<sup>35,36</sup>. Neither of these two possibilities would obviate the importance of the relevant frequencies to interregional communication, but they would affect the interpretation of how changes in the phase locking at these frequencies result from stimulus processing. In order to definitively resolve this ambiguity between interregional



coupling and local power, new methods will need to be developed and tested to assess phase locking independent of local power changes. Finally, we only compared stimulus-driven and spontaneous synchrony in two, relatively low-level sensory systems. Further studies will be required to determine whether the frequency correspondence between spontaneous and stimulus driven activity is a general property of the brain, particularly for higher-level networks.

Our findings provide evidence that, at the level of large-scale neural interactions, spontaneous neural synchrony has a coherent temporal structure, with the nodes of different networks showing preferential biases for interacting within limited frequency bands. They further suggest that frequency-specific oscillatory dynamics are intrinsic to the interactions between the nodes of these brain networks. These dynamics can potentially be tied to specific biological and functional properties of neurons and networks<sup>13,37–40,49</sup>. Therefore, a better understanding of intrinsic dynamics and how they are altered in pathological conditions may yield critical insights into the mechanisms behind spontaneous oscillatory synchrony and abnormalities of functional connectivity.

## Methods

**Subjects.** A total of 15 individuals participated in the experiments. One subject was excluded due to unusually large cardiac and respiratory artifacts and another subject was excluded due to head movement in excess of .5 cm, thus 13 subjects were included in the analysis (8 males, mean age = 27.3, SD = 8.1). Of these 13 subjects, seven individuals participated in both of the stimulus-driven experiments and six individuals participated in just one of the two stimulus-driven experiments (a total of 10 subjects in each experiment). Spontaneous activity was recorded from all subjects. All subjects were naive to the goals of the study. The Institutional Review Board of the National Institutes of Health approved all procedures and written informed consent was obtained for all subjects.

**Recording.** Neuromagnetic responses were recorded at 600 Hz using a 275 channel whole head MEG system in a shielded room (VSM MedTech, Ltd., Canada). The magnetometer is equipped with 275 radial gradiometers (273 were functional) and synthetic 3<sup>rd</sup> order gradient noise cancellation was used. Head position coils were placed at the nasion and left and right preauricular points to coregister the anatomical MRI and the MEG sensors. Head position was determined at the beginning and end of each run to ensure that head movements did not exceed .5 cm for any subject. Eyeblinks and eye movements were recorded using a bi-polar EOG electrode placed about each subject's left eye.

**Structural MRI.** Structural MRI images were obtained separately using a 3-Tesla whole-body scanner (GE Signa, USA). A high-resolution T1-weighted 3D volume was obtained for each subject. Freesurfer<sup>TM</sup> was used to create a cortical surface model for each subject using an automatic reconstruction algorithm. The cortical white matter was segmented providing a topologically correct representation of the surface with approximately 150,000 vertices per hemisphere. The cortical surface was then decimated to approximately 4,000 source dipoles per hemisphere, approximately 1 dipole every 10 mm along the cortical surface. The MEG data were coregistered with anatomical MR images using fiducial headpoints.

**Behavioral tasks.** Each subject first participated in a 12 minute scan of spontaneous activity where their task was to fixate on a centrally presented cross. Subjects were not given any details about later tasks during this scan. Following the recording of spontaneous activity, the subjects were presented with a series of button-press trials. Every 2 seconds, a white fixation cross in the middle of the screen would change to green or purple for 200 ms. The subjects were instructed to press a button with their left index finger when the cross turned green and a different button with their right index finger when the cross turned purple. The subjects were presented with 100 trials in each condition. Following this task, the subjects were presented with a series of auditory clicks trials binaurally using MEG compatible ear buds. Each trial consisted of 500 ms of a 1910 Hz pure tone modulated by square waves at 15, 20, 30, or 40 Hz followed by 1500 ms of silence. The subjects were presented with 100 trials of each frequency and asked only to fixate on a centrally presented cross throughout the experiment.

**MEG analysis. Artifact removal.** For artifact removal, we first visually inspected the data for any respiratory artifacts. These artifacts are generally uncommon in MEG data, particularly with the use of third-order gradiometer compensation. However, if subjects accidentally have metal on or in their persons these artifacts can be substantial (one subject in our study was excluded for this reason). We then used a short-time Fast Fourier filter to band-pass the data between 1 and 50 Hz (the filter uses the overlap-add technique with a time window of 4096, the highpass transition width is 0.0 Hz and the lowpass transition width is 5.0 Hz). This removed low frequency drift, any residual respiratory artifact, 60 Hz line noise, and any DC offset.

Cardiac artifacts were removed using an independent component analysis-based procedure following Liu et al.<sup>52</sup>. Briefly, the MEG sensor data were decomposed into 273 independent components (ICs) using EEGLAB<sup>53</sup>. ICs were identified as being a cardiac artifact if the IC had a peak in its autocorrelation spectrum between .6–1.5 Hz (by observing whether there were regular peaks in the autocorrelation every 667–1667 ms), the IC had a timecourse that contained periodic features that were similar to those seen on an electrocardiogram, and had power in the MEG sensors that typically contain cardiac features. Across our subjects, between 1 and 3 cardiac ICs were rejected and the remaining ICs were reassembled for further processing.

To monitor ocular muscle activity we measured EOG along with the MEG measurements. The EOG timecourses were pseudo-Z transformed into standard deviation (SD) units (by subtracting the mean across the epoch and dividing by the SD). These data were visually inspected and the minimum size of each subject's eye blinks in these units was determined (mean = 1.67 [in SD units], min 1.5, max 2.0). Centered about each point that exceeded these thresholds, the data 300 ms before and 500 ms after these points were excluded from further analysis (on average this removed 1200 ms per eye blink). These additional windows of data were excluded so that sufficient pre- and post-artifact data were removed to ensure no artifacts remained in the analyzed timecourses. These conservative thresholds and windows removed on average 38% of the time points across subjects, leaving 7.4 minutes of artifact-free data on average. Note that simulations demonstrate that the discontinuities in the data created by this artifact removal procedure do not substantially affect the calculated phase locking above 3 Hz<sup>24</sup>.

**Inverse solution.** The exact location of the cortical current sources cannot be precisely determined using the measured magnetic fields from outside the head, and therefore it is estimated using cortically constrained minimum norm estimate (MNE), described extensively elsewhere<sup>54,55</sup>. Briefly, a linear inverse operator  $W$  is applied to the measured signal to calculate the MNE

$$y(t) = W x(t)$$

where  $x(t)$  represents the MEG channel data at time  $t$  and  $y(t)$  is the corresponding current projected onto the cortical surface. The expression of  $W$  is defined as

$$W = RA^T (ARA^T + \lambda^2 C)^{-1}$$

where  $C$  and  $R$  are the noise and source covariance matrices respectively.  $A$  defines the transformation from orthogonal unit current dipoles to measured magnetic fields and uses the boundary element method<sup>56,57</sup>.  $\lambda$  is a weighting factor that is used to avoid the magnification of errors in the data and  $\lambda^2 \approx (1/\text{SNR})$ . We used a value of 3 for this, as is typically done in MEG analysis (Hämäläinen, MNE software user's guide version 2.7, 2009). Furthermore, because cortical neurons are known to be preferentially oriented perpendicular to the cortical surface, we used a loose orientation constraint. Specifically, the component of  $R$  normal to the surface was multiplied by 1 and the components transverse to the surface was multiplied by 4. To compensate for the bias towards superficial currents of the MNE a scaling factor (i.e. depth weighting) of .8 is applied to  $R^2$ . The noise covariance matrix was calculated from 12 minutes of continuous empty room MEG measurements collected immediately prior to putting the subject in the scanner<sup>24</sup>.

To estimate the time course and statistical significance of the cortical MEG activity, noise normalized values were calculated at each time point and each dipole location<sup>55</sup>. This transforms power values into dynamic statistical parametric values (dSPM) and makes the point spread function of the estimated signal relatively uniform across cortical dipoles<sup>58</sup>. For ROI localization these dSPM values are used to describe the neural activity.

**ROI localization.** To localize LH primary motor cortex (LM1) and LH secondary somatosensory cortex (LS2), the locus of peak activity about the central sulcus occurring for activity averaged from 0 to 150 ms after subjects pressed the button with their left hand was calculated. This time period was chosen because the neural response at this time includes somatosensory activity in response to proprioception of the button press. To localize LM1 and LS2, the locus of peak activity about the central sulcus occurring for activity averaged from 0 to 150 ms after subjects pressed the button with their right hand was calculated. The portion of this activity anterior to the central sulcus, but posterior to the superior frontal gyrus and middle frontal gyrus, was used as the location of LM1 and the portion of the activity just ventral to the central sulcus extending into the dorsal insula, was used as the location of LS2 for each subject. This time period was chosen to correspond approximately to the proprioception in response to the button press. The portion of this activity anterior to the central sulcus was used as the location of the RM1 and the portion of this activity posterior to the central sulcus was used as the location of RS1 for each subject. Synchrony between RS1 and LS1 or between RS1 and RS2 could not be reliably evaluated due to the potential for artifactual cross-talk between locations less than 6 cm apart in MEG<sup>24</sup>.

To localize LH and RH auditory cortex (LAud and RAud), the activity between 50 and 550 ms after the onset of the auditory clicks was averaged. The peak of the activity within a 2 cm radius circle on the surface around Heschl's gyrus (determined based on anatomical landmarks provided by Freesurfer<sup>TM</sup>) was used as the location of the LAud and RAud ROI for each subject.

**Stimulus-driven phase locking analysis.** To determine the trial-by-trial phase locking between neural regions, we employed the dynamic spectral statistical



parametric mapping method<sup>22</sup>, a method to measure phase synchrony between signals projected onto the cortical surface. This method employs the anatomically constrained MNE inverse solution<sup>54,55</sup> to determine phase locking values (PLVs)<sup>25</sup> between regions on the cortical surface.

To calculate PLVs, the MEG sensor data were filtered using a continuous Morlet wavelet transform at each frequency of interest described by the equation:

$$G(t, f) = \frac{1}{\sqrt{2\pi f}} e^{\left(\frac{t-t_0}{\sigma}\right)^2} e^{2\pi i f t}$$

where  $\sigma$  is the SD of the Gaussian envelope of the wavelet in the time domain. To ensure stability of the wavelet transform here we set  $\sigma$  to be  $\frac{7}{2\pi f}$ . The wavelet

representation of each trial was then mapped from the sensors onto the cortex using the MNE inverse solution. The phase was then extracted from the wavelet data averaged across all dipoles in each region of interest for each trial about each time point and at each frequency of interest. Prior to averaging, the phases were rectified to correct for the sign inversion that occurs within large ROIs for due to crossing a sulcus or gyrus. Specifically, we iteratively flipped the sign of the dipoles in an ROI until no pair of dipoles showed strong negative correlations ( $r < -.3$ ). The PLV was then determined using the following formula:

$$PLV(t) = \frac{1}{N} \left| \sum_{n=1}^N \exp(j(\phi_1(t, n) - \phi_2(t, n))) \right|$$

where  $\phi(t, n)$  is the phase of the signals from the two ROIs at time  $t$  and trial  $n$ . PLVs range from 0 to 1, where 1 indicates perfect synchrony across trials and 0 indicates the phase relationship is completely random. The same timeframes used to select the ROIs from the evoked signal were used for the stimulus-driven PLVs and equal time windows from the prestim were used for prestimulus PLVs. Stimulus-driven PLVs were scaled by the PLV expected by chance calculated using the Rayleigh distribution.

**Spontaneous phase locking.** Spontaneous phase locking measures the variability over time of the phase difference between the seed and the other cortical locations<sup>24</sup>. Specifically, the spontaneous PLV is defined as:

$$PLV_i = \frac{1}{N} \left| \sum_{n=1}^N e^{j(\theta_{seed}(n) - \theta_i(n))} \right|$$

where  $N$  is the number of time points in the sample and  $\theta_{seed}(n)$  and  $\theta_i(n)$  are the phase of the wavelet convolved data in the seed ROI and the cortical locations “ $i$ ” respectively. Spontaneous PLVs were scaled by the PLV found in empty room noise as described in Ghuman et al. 2011<sup>24</sup>.

**The Fourier spectrum of spontaneous phase locking.** To assess the rate of change of the spontaneous phase locking, we first calculated the phase locking in 1 second, half-overlapping windows (i.e. the  $N$  in the equation above was 1 second for each window) to across the artifact free portion of the 12 minute spontaneous activity scan (e.g. figures 4a and 4c). This yielded a timecourse of the PLVs over the spontaneous activity scan. We then calculated the Fourier spectrum of this PLV timecourse in Matlab<sup>TM</sup>. 24 Hz was chosen for the RS1-LS2 interaction (18 Hz was chosen as a control frequency) and 10 Hz was chosen for the RAud-LAud interaction (20 Hz was chosen as a control frequency) because these were the frequencies that showed the greatest spontaneous phase locking relative to baseline (see figures 2b and 3b). The procedure above was then performed on 1000 simulations of Gaussian distributed random data to estimate the time-windowed PLVs and Fourier spectra in noise. The fit of the Fourier spectrum of the resting-state and noise PLV timecourses to a line and a  $1/f$  curve using a least squares fit was determined.

In addition to calculating the phase locking in these windows, we calculated the local power in RS1 and LS2 at 24 and 18 Hz, and RAud and LAud at 10 and 20 Hz by taking the absolute value of the wavelet transformed response in each region. We then calculated the correlation between these local power time courses and the phase locking time courses described in the previous paragraph. This allowed us to examine the potential effect of local power changes over time on the interregional phase locking<sup>35,36</sup>.

**Statistics.** Nonparametric statistics were then used to compare conditions and control for multiple comparisons<sup>26</sup>. All the frequency points that were  $p < .05$  for the prestimulus vs. the poststimulus periods were determined and clustered on the basis of frequency adjacency. Cluster level statistics were calculated by determining the sum of the  $t$ -values within each cluster (cluster mass) and the maximum cluster mass across the data was determined. Permutations were then created by collecting the data from the prestimulus and task conditions across the 10 subjects in a single set. Half of these collected trials were placed into subset one and the remaining were placed into subset two. The maximum cluster mass was then determined for all possible permutations of the data ( $2^9$  partitions for 10 subjects). The proportion of these permutations that had a smaller maximum cluster mass than the non-permuted data was the  $p$ -value calculated using a complete permutation test. Because of the global null hypothesis used for the cluster mass test, this method inherently controls for multiple comparisons.

For the spontaneous phase locking analysis, two partitions were formed based on the ROI pair of interest and the control ROI pair comparison (i.e. for the first experiment, RS1-LS2 were the ROI pair of interest and RM1-LS2 was the control ROI

pair, for the second experiment LAud-RAud were the ROI pair of interest and LM1-RAud were the control ROI pair). All the frequency points that were  $p < .05$  for two separate criteria were determined: 1. the ROI pair of interest vs. the control 2. the ROI pair of interest vs. the PLV for the ROI pair of interest in noise<sup>24</sup>. These frequency points were then clustered on the basis of frequency adjacency and the rest of the statistics followed the procedure laid out above.

1. Fox, M. D., Snyder, A. Z., Vincent, J. L. & Raichle, M. E. Intrinsic fluctuations within cortical systems account for intertrial variability in human behavior. *Neuron* **56**, (2007).
2. Carr, M. F., Jadhav, S. P. & Frank, L. M. Hippocampal replay in the awake state: a potential substrate for memory consolidation and retrieval. *Nature Neuroscience* **14**, 147–153 (2011).
3. Blankenship, A. G. & Feller, M. B. Mechanisms underlying spontaneous patterned activity in developing neural circuits. *Nature Rev Neurosci* **11**, 18–29 (2010).
4. Berkes, P., Orban, G., Lengyel, M. & Fiser, J. Spontaneous cortical activity reveals hallmarks of an optimal internal model of the environment. *Science* **331**, 83–87 (2011).
5. Fiser, J., Chiu, C. & Weliky, M. Small modulation of ongoing cortical dynamics by sensory input during natural vision. *Nature* **431**, 573–578 (2004).
6. Kenet, T., Bibitchkov, D., Tsodyks, M., Grinvald, A. & Arieli, A. Spontaneously emerging cortical representations of visual attributes. *Nature* **425**, 954–956 (2003).
7. Luczak, A., Bartho, P. & Harris, K. D. Spontaneous Events Outline the Realm of Possible Sensory Responses in Neocortical Populations. *Neuron* **62**, 413–425 (2009).
8. Tsodyks, M., Kenet, T., Grinvald, A. & Arieli, A. Linking spontaneous activity of single cortical neurons and the underlying functional architecture. *Science* **286**, 1943–1946 (1999).
9. Rosanova, M. et al. Natural frequencies of human corticothalamic circuits. *J Neurosci* **29**, 7679–7685 (2009).
10. Fiser, J., Berkes, P., Orban, G. & Lengyel, M. Statistically optimal perception and learning: from behavior to neural representations. *Trends Cogn Sci* **14**, 119–130 (2010).
11. Lakatos, P. et al. An oscillatory hierarchy controlling neuronal excitability and stimulus processing in the auditory cortex. *J Neurophys* **94**, 1904–1911 (2005).
12. Biswal, B., Yetkin, F. Z., Haughton, V. M. & Hyde, J. S. Functional connectivity in the motor cortex of resting human brain using echo-planar MRI. *Magn Reson Med* **34**, 537–541 (1995).
13. Fox, M. D. & Raichle, M. E. Spontaneous fluctuations in brain activity observed with functional magnetic resonance imaging. *Nature Rev Neurosci* **8**, 700–711 (2007).
14. Simmons, W. K. & Martin, A. Spontaneous resting-state BOLD fluctuations reveal persistent domain-specific neural networks. *Soc Cogn Affect Neurosci* **7**, 467–475 (2012).
15. Vincent, J. L. et al. Intrinsic functional architecture in the anaesthetized monkey brain. *Nature* **447**, 83–86 (2007).
16. He, B. J., Snyder, A. Z., Zempel, J. M., Smyth, M. D. & Raichle, M. E. Electrophysiological correlates of the brain’s intrinsic large-scale functional architecture. *Proc Natl Acad Sci U S A* **105**, 16039–16044 (2008).
17. Leopold, D. A., Murayama, Y. & Logothetis, N. K. Very slow activity fluctuations in monkey visual cortex: implications for functional brain imaging. *Cereb Cortex* **13**, 422–433 (2003).
18. Nir, Y. et al. Interhemispheric correlations of slow spontaneous neuronal fluctuations revealed in human sensory cortex. *Nat Neurosci* **11**, 1100–1108 (2008).
19. de Pasquale, F. et al. A cortical core for dynamic integration of functional networks in the resting human brain. *Neuron* **74**, 753–764 (2012).
20. Hipp, J. F., Hawellek, D. J., Corbetta, M., Siegel, M. & Engel, A. K. Large-scale cortical correlation structure of spontaneous oscillatory activity. *Nature Neurosci* (2012).
21. Montgomery, S. M., Betancur, M. I. & Buzsaki, G. Behavior-dependent coordination of multiple theta dipoles in the hippocampus. *J Neurosci* **29**, 1381–1394 (2009).
22. Lin, F. H. et al. Spectral spatiotemporal imaging of cortical oscillations and interactions in the human brain. *Neuroimage* **23**, 582–595 (2004).
23. Simoes, C., Jensen, O., Parkkonen, L. & Hari, R. Phase locking between human primary and secondary somatosensory cortices. *Proc Natl Acad Sci U S A* **100**, 2691–2694 (2003).
24. Ghuman, A. S., McDaniel, J. R. & Martin, A. A wavelet-based method for measuring the oscillatory dynamics of resting-state functional connectivity in MEG. *Neuroimage* (2011).
25. Lachaux, J. P., Rodriguez, E., Martinerie, J. & Varela, F. J. Measuring phase synchrony in brain signals. *Hum Brain Mapp* **8**, 194–208 (1999).
26. Maris, E. & Oostenveld, R. Nonparametric statistical testing of EEG- and MEG-data. *J Neurosci Methods* **164**, 177–190 (2007).
27. Baker, S. N., Kilner, J. M., Pinches, E. M. & Lemon, R. N. The role of synchrony and oscillations in the motor output. *Exp Brain Res* **128**, 109–117 (1999).
28. Baker, S. N., Olivier, E. & Lemon, R. N. Coherent oscillations in monkey motor cortex and hand muscle EMG show task-dependent modulation. *J Physiol* **501** (Pt1), 225–241 (1997).



29. Roopun, A. K. *et al.* A beta2-frequency (20–30 Hz) oscillation in nonsynaptic networks of somatosensory cortex. *Proc Natl Acad Sci U. S. A.* **103**, 15646–15650 (2006).
30. Salmelin, R. & Hari, R. Spatiotemporal characteristics of sensorimotor neuromagnetic rhythms related to thumb movement. *Neuroscience* **60**, 537–550 (1994).
31. Lehtela, L., Salmelin, R. & Hari, R. Evidence for reactive magnetic 10-Hz rhythm in the human auditory cortex. *Neurosci Lett* **222**, 111–114 (1997).
32. Schürmann, M., Basar-Eroglu, C. & Basar, E. A possible role of evoked alpha in primary sensory processing: Common properties of cat intracranial recordings and human EEG and MEG. *Int J Psychophysiol* **26**, 149–170 (1997).
33. van Dijk, H., Nieuwenhuis, I. L. C. & Jensen, O. Left temporal alpha band activity increases during working memory retention of pitches. *European J Neurosci* **31**, 1701–1707 (2010).
34. Brookes, M. J. *et al.* Investigating the electrophysiological basis of resting state networks using magnetoencephalography. *Proc Natl Acad. Sci U. S. A.* **108**, 16783–16788 (2011).
35. Ghuman, A. S., McDaniel, J. R. & Martin, A. Differences in connectivity or differences in signal-to-noise ratio? In *Organization for Human Brain Mapping* (San Francisco, 2009).
36. Muthukumaraswamy, S. D. & Singh, K. D. A cautionary note on the interpretation of phase-locking estimates with concurrent changes in power. *Clin Neurophysiol* **122**, 2324–2325 (2011).
37. Kopell, N., Ermentrout, G. B., Whittington, M. A. & Traub, R. D. Gamma rhythms and beta rhythms have different synchronization properties. *Proc Natl Acad Sci U S A* **97**, 1867–1872 (2000).
38. Kopell, N., Kramer, M. A., Malerba, P. & Whittington, M. A. Are different rhythms good for different functions? *Front Hum Neurosci* **4**, 187 (2010).
39. Hutcheon, B. & Yarom, Y. Resonance, oscillation and the intrinsic frequency preferences of neurons. *Trends Neurosci* **23**, 216–222 (2000).
40. Llinas, R. R. The intrinsic electrophysiological properties of mammalian neurons: insights into central nervous system function. *Science* **242**, 1654–1664 (1988).
41. Roopun, A. K. *et al.* Cholinergic neuromodulation controls directed temporal communication in neocortex in vitro. *Front Neural Circuits* **4**, 8 (2010).
42. Sauseng, P. *et al.* Are event-related potential components generated by phase resetting of brain oscillations? A critical discussion. *Neuroscience* **146**, 1435–1444 (2007).
43. Makeig, S. *et al.* Dynamic brain sources of visual evoked responses. *Science* **295**, 690–694 (2002).
44. Fries, P., Reynolds, J. H., Rorie, A. E. & Desimone, R. Modulation of oscillatory neuronal synchronization by selective visual attention. *Science* **291**, 1560–1563 (2001).
45. Jutras, M. J., Fries, P. & Buffalo, E. A. Gamma-band synchronization in the macaque hippocampus and memory formation. *J Neurosci* **29**, 12521–12531 (2009).
46. Tallon-Baudry, C., Bertrand, O. & Fischer, C. Oscillatory synchrony between human extrastriate areas during visual short-term memory maintenance. *J Neurosci* **21**, RC177 (2001).
47. Canolty, R. T. *et al.* High gamma power is phase-locked to theta oscillations in human neocortex. *Science* **313**, 1626–1628 (2006).
48. Tort, A. B. *et al.* Dynamic cross-frequency couplings of local field potential oscillations in rat striatum and hippocampus during performance of a T-maze task. *Proc Natl Acad Sci U. S. A.* **105**, 20517–20522 (2008).
49. Tabareau, N., Slotine, J. J. & Pham, Q. C. How synchronization protects from noise. *PLoS Comput Biol* **6**, e1000637 (2010).
50. Handwerker, D. A., Roopchansingh, V., Gonzalez-Castillo, J. & Bandettini, P. A. Periodic changes in fMRI connectivity. *Neuroimage* **63**, 1712–1719 (2012).
51. Chang, C. & Glover, G. H. Time-frequency dynamics of resting-state brain connectivity measured with fMRI. *Neuroimage* **50**, 81–98 (2010).
52. Liu, Z., Fukunaga, M., de Zwart, J. A. & Duyn, J. H. Large-scale spontaneous fluctuations and correlations in brain electrical activity observed with magnetoencephalography. *Neuroimage* **51**, 102–111 (2010).
53. Delorme, A. & Makeig, S. EEGLAB: an open source toolbox for analysis of single-trial EEG dynamics including independent component analysis. *J Neurosci Methods* **134**, 9–21 (2004).
54. Hamalainen, M. S. & Hari, R. In *Brain Mapping: The Methods* (eds Toga, A. V. & Mazziotta, J. C.) 227–254 (Academic Press, 2002).
55. Dale, A. M. *et al.* Dynamic statistical parametric mapping: combining fMRI and MEG for high-resolution imaging of cortical activity. *Neuron* **26**, 55–67 (2000).
56. Hamalainen, M. S. & Sarvas, J. Realistic Conductivity Geometry Model of the Human Head for Interpretation of Neuromagnetic Data. *Ieee T Bio-Med Eng* **36**, 165–171 (1989).
57. Oostendorp, T. F. & Vanoosterom, A. Source Parameter-Estimation in Inhomogeneous Volume Conductors of Arbitrary Shape. *Ieee T Bio-Med Eng* **36**, 382–391 (1989).
58. Liu, A. K., Dale, A. M. & Belliveau, J. W. Monte Carlo simulation studies of EEG and MEG localization accuracy. *Human Brain Mapping* **16**, 47–62 (2002).

## Acknowledgments

We thank Jonathan McDaniel for assistance with data collection, Steve Gotts, Dale Stevens, David Leopold, and Alex Maier for insightful comments, and Tom Holroyd and the staff NIMH MEG core for assistance with data collection. This work was supported by the NIMH-DIRP.

## Author contributions

A.S.G. and A.M. designed the study; A.S.G. and R.v.d.H. collected the data; A.S.G., R.v.d.H. and A.M. wrote and reviewed the manuscript.

## Additional information

**Competing financial interests:** The authors declare no competing financial interests.

**License:** This work is licensed under a Creative Commons Attribution-NonCommercial-NoDerivs 3.0 Unported License. To view a copy of this license, visit <http://creativecommons.org/licenses/by-nc-nd/3.0/>

**How to cite this article:** Ghuman, A.S., van den Honert, R.N. & Martin, A. Interregional neural synchrony has similar dynamics during spontaneous and stimulus-driven states. *Sci Rep.* **3**, 1481; DOI:10.1038/srep01481 (2013).